Journal of Zhejiang University-SCIENCE A (Applied Physics & Engineering)
ISSN 1673-565X (Print); ISSN 1862-1775 (Online)
www.jzus.zju.edu.cn; www.springerlink.com
E-mail: jzus@zju.edu.cn

Surface settlements induced by tunneling in permeable strata: a case history of Shenzhen Metro*

Xiao-wu TANG[1], Peng-lu GAN[1,2], Wei LIU[3], Yu ZHAO[†‡4]

([1]*Research Center of Coastal and Urban Geotechnical Engineering, Zhejiang University, Hangzhou 310058, China*)

([2]*PowerChina Huadong Engineering Corporation Limited, Hangzhou 311122, China*)

([3]*School of Urban and Rail Transit, Soochow University, Suzhou 215137, China*)

([4]*Institute of Disaster Prevention Engineering, Hangzhou 310058, China*)

[†]E-mail: zhao_yu@zju.edu.cn

Received July 20, 2016; Revision accepted Dec. 16, 2016; Crosschecked Sept. 7, 2017

Abstract: A case study of a significant surface settlement induced by tunneling in permeable strata with the shallow tunneling method is presented in this paper. The measurements of surface settlements along the excavation direction were first analyzed to highlight the impacts of groundwater seepage. Due to the groundwater inflow inside a double-arched tunnel, the surface settlement developed to a high level far beyond the measured crown settlement. The settlement-affected zone extended to 4 times the tunnel height ahead of the forefront heading and 1.5 times the tunnel height behind the hindmost heading. Consolidation resulting from high pore pressure change was considered to be the main mechanism for the large surface settlements. In addition, a 3D fluid-mechanical coupled numerical analysis was carried out to confirm the relationship between the significant surface settlement and pore pressure variation. This analysis reveals that lowering the permeability of the small pipe grouting zone, especially of the primary lining, could lessen the drop in pore pressure in the overlying strata, further reducing the total surface settlement. The numerical results also suggest that the transverse range of vertical displacement could be quite wide, and the settlement developed integrally from the tunnel crown towards the ground surface due to groundwater seepage. Moreover, the effect of advance drainage on surface settlement was investigated based on the same numerical model. Drainage with horizontal boreholes could considerably increase the safety of tunnel heading but had limited impact on surface settlement. Finally, the applications of pre-grouting and advance drainage measures were discussed for tunneling cases in permeable strata.

Key words: Surface settlement; Shallow tunneling method (STM); Groundwater seepage; Pre-grouting; Advance drainage; Fluid-mechanical coupled analysis

http://dx.doi.org/10.1631/jzus.A1600522 **CLC number:** U455

1 Introduction

As the urban population in China has greatly expanded over the last two decades, especially in some metropolises such as Beijing, Shanghai, and Shenzhen, an increasing number of subway and road tunnels have been constructed to alleviate traffic pressure. Currently, one main tunneling technique in urbanized areas of China is the shallow tunneling method (STM), which was first applied to the Jundushan Tunnel in 1984 (Wang, 2010). This method was developed from the new Austrian tunneling method (NATM), which is used for tunnel construction worldwide. However, the design philosophies underlying the STM and the NATM are different; the STM requires short excavation lengths and quick primary support rather than mobilizing the

‡ Corresponding author

* Project supported by the National Natural Science Foundation of China (No. 51508503), the Fund of the China Scholarship Council (No. 201406320025), and the Research Plan of the Academician Workstation of Guangzhou Chemical Grouting Co. Ltd., China Academy of Science (No. 2016GZZ01)

ORCID: Yu ZHAO, http://orcid.org/0000-0003-0453-1960

strength of the ground as much as possible. In addition, pre-reinforcement, such as pre-grouting or a pipe roof, is mandatory to achieve shallow tunneling in soft ground. Fang *et al*. (2012) summarized the following two mechanical characteristics of the STM: (1) limited ground strength mobilization and (2) limited arching effect.

Ground deformation has always been one of the most concerning problems in the use of the STM because excessive ground settlement causes damage to buildings, buried pipelines, and other existing structures close to the tunneling route. In general, tunneling-induced settlement is primarily related to the amount of ground convergence into the excavation region of tunnels, which is also known as "volume loss". Volume loss can be mainly divided into face loss and radial loss around the tunnel periphery (Attewell *et al*., 1986). The magnitude of the volume loss is dependent on the tunneling method, geological conditions, and quality of workmanship (Mair, 1996). Based on extensive field measurements of settlements, empirical formulas were proposed for predicting surface settlement due to volume loss (Peck, 1969; Attewell and Woodman, 1982; New and O'Reilly, 1991). For two or more tunnels excavated in close proximity, the validity of the superposition of Gaussian functions in describing transverse surface settlement troughs has been verified in different tunnel projects (Suwansawat and Einstein, 2007; Chen *et al*., 2012). Chapman *et al*. (2007) also introduced a method that modified the Gaussian function to predict ground movement associated with twin tunnels by carrying out a series of model tests. Moreover, numerical analysis has been a popular tool to predict surface settlement for both mechanized tunneling and conventional tunneling, as it can handle almost all complicated engineering conditions (de Farias *et al*., 2004; Ercelebi *et al*., 2011; Do *et al*., 2014).

When tunneling in permeable strata, groundwater inflow is likely to occur and consequently influence the hydraulic head in soil layers (Anagnostou, 1995). Consolidation deformation will occur as a result of the reduction of pore water pressures and redistribution of effective stresses in the strata, which enlarges the value of volume loss. By establishing 3D stress-pore pressure coupled finite element analyses, Yoo (2005) investigated the influence of relative permeability between linings and surrounding soil on the surface settlement and horizontal displacement. Moreover, Anagnostou (2008) investigated the effect of the ratio of advance rate to ground permeability on the surface settlement by the use of numerical analysis. Yoo *et al*. (2012) presented a case history of conventional tunneling in Korea in which excessive ground surface settlement caused by groundwater drawdown was discovered. Although the settlement problems caused by ground convergence and groundwater seepage have been highlighted, research on surface settlement with regard to the STM is quite limited (Xiang *et al*., 2005; Fang *et al*., 2011; Liu *et al*., 2016), which exposes practical tunneling to potential operation risks in controlling surface settlement.

In Shenzhen, approximately 30% of the rail transit projects in the region with a high groundwater level were constructed with the STM. The maximum volume loss reached 9.2% (Zhang *et al*., 2008). This paper presents one project case of Shenzhen Metro during which significant surface settlement occurred during the construction of multiple tunnels in permeable strata. The measured ground surface settlements were first analyzed with the process of tunneling to highlight the adverse impacts of groundwater seepage. Surface settlements were subsequently compared with the measured crown settlements. Finally, a 3D fluid-mechanical coupled analysis was carried out using the finite difference program FLAC^{3D}. The influences of the permeability of the pre-grouting zone and primary lining on the surface settlement were studied, and a common tunneling condition using advance horizontal drainage boreholes was investigated.

2 Project background

2.1 General information

The project is located in the eastern area of Shenzhen surrounded by dense residential blocks and commercial buildings, where Huanzhong Line overlies Xili Line of Shenzhen Metro. The upper Huanzhong Line is designed to be a double-arched tunnel with a transition to twin arched tunnels along the excavation direction, whereas the lower Xili Line is composed of twin arched tunnels consistently (Fig. 1). The intersection angle between the two lines is very small. The two lines start from the No. 2 shaft

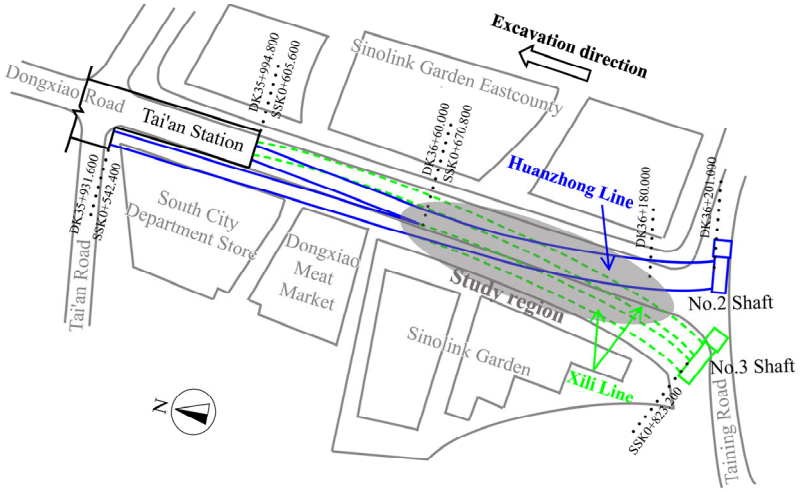

Fig. 1 Plan of project site

and the No. 3 shaft, and both extend approximately 280 m to Tai'an Station. The section from DK36+180 to DK36+60, where Huanzhong Line remains to be a double-arched tunnel with a considerably large span, was selected to be the study region in this paper.

A typical transverse profile of the study region is shown in Fig. 2 (DK36+90). Huanzhong Line has an excavation width and height of approximately 12.3 m and 7.1 m, respectively, with a cover depth of 15.2 m. The width and height of Xili Line beneath are approximately 6.3 m and 6.5 m, respectively. The soil thickness between the two lines is 1 m on average and reaches a minimum value of 0.9 m near DK36+170. Fig. 3 plots a typical longitudinal profile of the stacked section. The inclination of both Huanzhong Line and Xili Line is 5% in the study region.

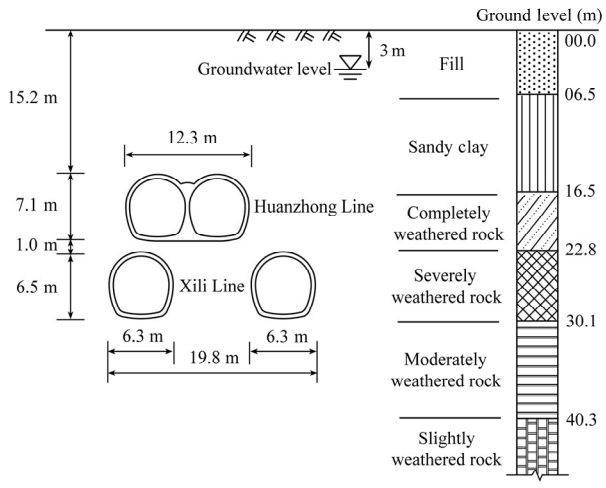

Fig. 2 Typical transverse profile (not to scale)

Huanzhong Line is constructed in composited layers including sandy clay and completely weathered rock, and Xili Line lies mainly on the ground of severely weathered rock.

2.2 Ground conditions

As shown in Fig. 3, the top layer is a 3–5 m thick artificial fill of quaternary Holocene with a blow count of N=6–11 according to a standard penetration test (SPT). The underlying quaternary Holocene eluvium (sandy clay) is 9–12 m thick. The N value of the sandy clay varies from 7 to 12. The layer below the sandy clay is Sinian migmatite that mainly contains quartz, feldspar, and mica. According to the weathering degree, the Sinian migmatite layer can be divided into the following four sublayers: completely (N=16–49), severely (N=42–60), moderately, and slightly weathered rocks in descending order. Based on the Chinese rock classification standard TB 10003-2005 (MOR, 2005), the four sublayers of migmatite can also be classified as Types V, V, VI, and III.

A high groundwater level ranges from 1.9 m to 3.9 m beneath the ground surface in the strata of the study region. The groundwater generally flows from north to south, and precipitation is the major source of supplementing groundwater. The permeability of the completely and severely weathered rock is relatively higher than the underlying sublayers. *In-situ* and laboratory tests have been conducted to obtain the geotechnical parameters of each layer, which are summarized in Table 1.

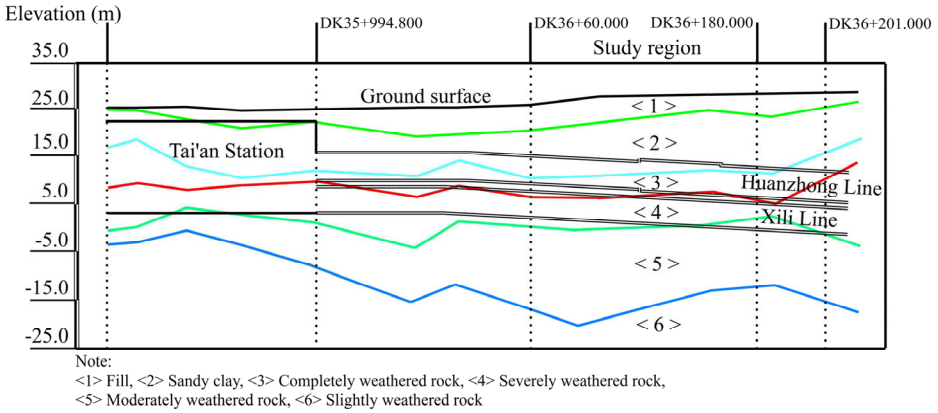

Fig. 3 Typical longitudinal profile (not to scale)

Table 1 Geotechnical parameters of soil layers

Soil type	Saturated unit weight, γ (kN/m^3)	Porosity, n	Young's modulus, E (MPa)	Poisson's ratio, v	Cohesion, c' (kPa)	Internal friction angle, φ' (°)	Dilatancy angle, ψ (°)	Vertical permeability coefficient, k (m/s)
1 Fill	18.1	0.40	5	0.20	17.6	18.2	0	6.5×10^{-6}
2 Sandy clay	18.9	0.45	8	0.31	26.9	23.0	0	4.6×10^{-7}
3 Completely weathered rock	19.1	0.43	12	0.30	28.0	24.5	0	3.8×10^{-6}
4 Severely weathered rock	19.2	0.41	30	0.27	29.0	27.2	0	1.2×10^{-6}
5 Moderately weathered rock	24.8	0.30	60	0.30	60.0	35.0	5	8.7×10^{-7}
6 Slightly weathered rock	26.6	0.15	120	0.30	100.0	40.0	10	4.0×10^{-8}

2.3 Construction schemes

The STM was applied to construct the overlapped tunnel lines. Specifically, the mid-pilot drift method was adopted for the upper Huanzhong Line, and the lower Xili Line was constructed with the simpler bench-cut method. The referred construction patterns are graphed in Fig. 4. As shown, the excavation of Huanzhong Line was divided into three the following sequential sections: first the middle pilot tunnel, then the left main tunnel and the right main tunnel. For each tunnel heading, two rows of advance small pipes (4 m in length) were installed above the crown for pre-grouting. The lap length between the two neighboring groups of small pipes was approximately 2 m in the excavation direction. The injected grout consists of cement and sodium silicate mixed with a small amount of retarder (Na_2HPO_4). Afterwards, each tunnel was excavated and primarily supported using the bench-cut method with a bench length of 3–5 m. It is worth mentioning that the tunnel heading was also sprayed with concrete to improve the heading stability. The length of one excavation cycle was approximately 2–2.5 m. The distance between two neighboring top headings was approximately 8–12 m with the middle pilot in the forefront. Additionally, the middle pillar, which is a portion of the secondary lining, was cast in advance before the excavation of the left tunnel.

For Xili Line, a particular advance full-section grouting was applied through numerous grouting pipes for the purpose of preventing groundwater from flowing inside. The length of one circulation of full-section grouting was 12 m, and the lap length between two adjacent circulations was approximately 2 m. With the assistance of this pre-grouting method, the weathered rock inside and approximately 2 m outside the periphery of the arched tunnels was reinforced and sealed in the cross section. The bench length was maintained at 3–5 m during the bench-cut tunneling. The detailed parameters of all support patterns are listed in Table 2.

To shorten the construction period, Huanzhong Line and Xili Line were designed to be constructed simultaneously with the rate of approximately 1.0 m/d. Relevant experience of simultaneous tunneling is quite insufficient owing to the lack of similar previous construction cases. For two stacked tunnels

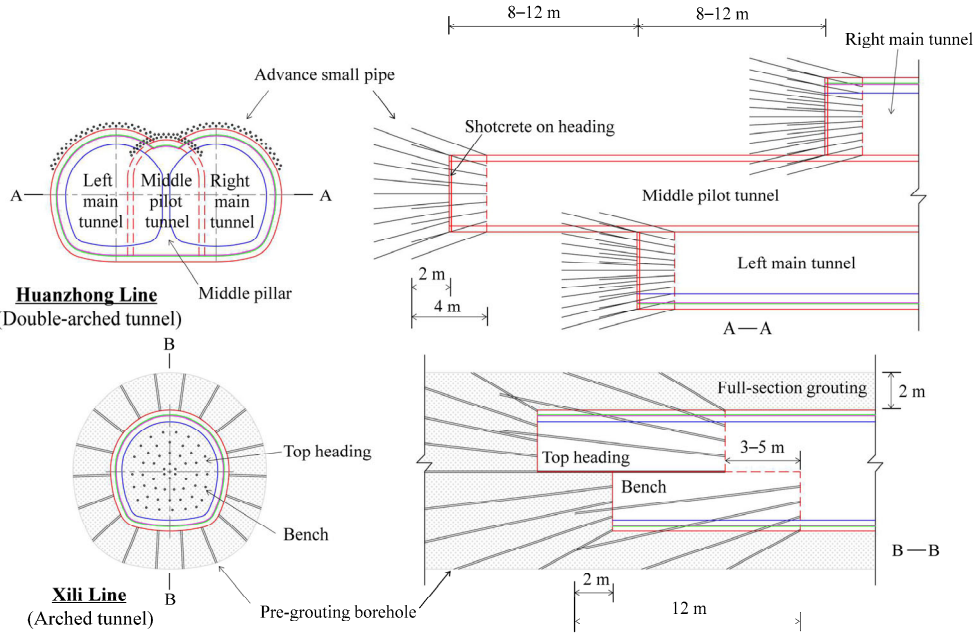

Fig. 4 Construction patterns of the tunnel lines

Table 2 Summary of the support patterns

Item		Description
Huanzhong Line	Small pipe grouting	Length: 4 m; Φ42 mm; Thickness: 3.5 mm; Cover zone: 120°; Incline: 5°–10°; Circumferential spacing: 333 mm; Lap length: 2.0 m; Grouting pressure: 0.4–0.6 MPa
	Primary support	Steel mesh: Φ8 mm@150 mm×150 mm, double layer
		Steel lattice: longitudinal spacing of 0.5 m
		Shotcrete: C25; Thickness: 0.3 m periphery, 0.06 m heading
	Secondary lining	Reinforced concrete: C30; Thickness: 0.45 m
Xili Line	Full-section grouting	Borehole: Φ42 mm; Cycle length: 12 m; Lap length: 2 m; Grouting pressure: 1–1.5 MPa
	Primary support	Steel mesh: Φ8 mm@150 mm×150 mm
		Steel lattice: longitudinal spacing of 0.75 m
		Shotcrete: C25; Thickness: 0.25 m
	Secondary lining	Reinforced concrete: C30; Thickness: 0.35 m

that are excavated successively, the excavation sequence that constructs the lower tunnel first and then the upper tunnel has been proved by numerical studies to be effective in controlling deformation and ensuring structural stability (Hefny *et al*., 2004; Hage Chehade and Shahrour, 2008). Therefore, this construction sequence was adopted for simultaneous tunneling with all tunnel headings separated by some distance, as shown in Fig. 5. Regarding Xili Line, the top heading of the west tunnel was approximately 12 m ahead of that of the east tunnel. Furthermore, a secure distance of 24 m between the bottom heading of the west tunnel of Xili Line and the top heading of the middle pilot tunnel of Huanzhong Line was determined by an onsite test tunneling section.

3 Settlement measurements and discussion

3.1 General information

The surface monitoring points in the study region were arranged in two lines, A and B, as shown in Fig. 6. Line A was installed upon Huanzhong Line and the east tunnel of Xili Line in the north–south direction, and line B was fixed along the excavation direction of the west tunnel of Xili Line. Judged from the location of the monitoring points with respect to the tunnels, the measurements from line A reflect the

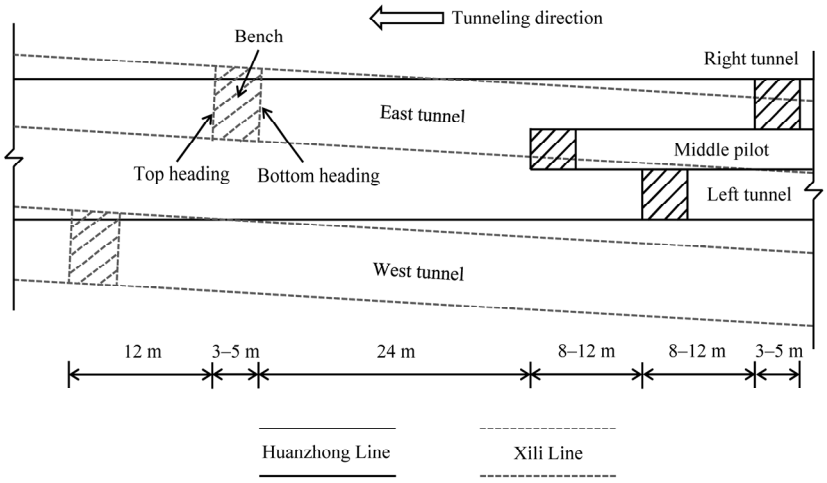

Fig. 5 Distances between tunnel headings

surface settlement induced by simultaneous tunneling more accurately. Therefore, line A was chosen for the following analysis. Line A consists of 13 monitoring points with an interval of 10 m, named from GS-1 to GS-13. The measurements of surface settlement lasted 116 d from Sept. 7 to Dec. 31, 2009, with a frequency of once per day. In addition, crown settlements were also measured in various cross sections located approximately 6–10 m apart (Fig. 6). The monitoring of the crown settlement was conducted after the construction of the primary lining, which means that the crown settlement that occurred before the completion of the primary lining is not included.

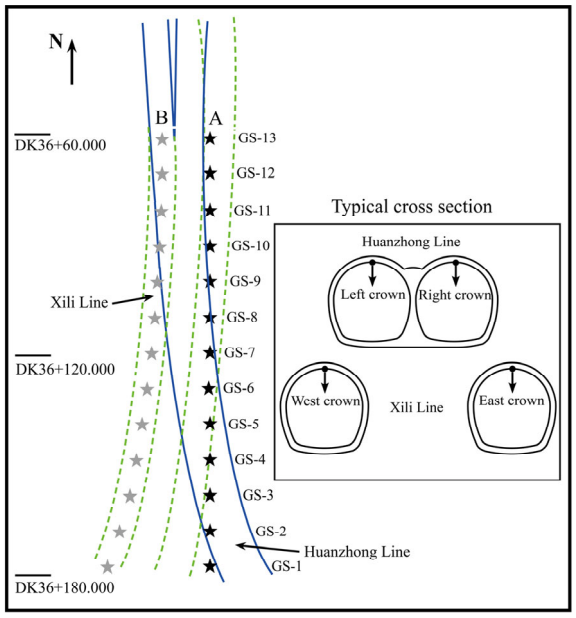

Fig. 6 Layout of monitoring points

3.2 Longitudinal surface settlements

Fig. 7 plots the surface settlements in the longitudinal direction every half-month. The initial positions of the top headings of the three tunnels are also indicated in Fig. 7, approximately DK36+92 for the west tunnel of Xili Line, DK36+104 for the east tunnel of Xili Line, and DK36+132 for the middle pilot tunnel of Huanzhong Line. Based on the initial positions of the tunnel headings, the surface settlements obtained from GS-1 to GS-6 can be roughly regarded as post-construction settlement and those from GS-7 to GS-13 are considered as construction settlement. During the monitoring period, the tunneling process was temporarily ceased until Sept. 27 owing to a severe groundwater leakage problem inside Huanzhong Line. Because the settlements before the stoppage were not measured, there was an evident turning point in the longitudinal settlement trough at the position of GS-6. The construction settlements were much larger than the post-construction settlements and kept increasing as the monitoring time went by.

The tunneling-induced settlement from GS-7 to GS-13 increased noticeably as time went by. The monitoring point that experienced the maximum half-month increment is indicated with a rectangle in Fig. 7. Meanwhile, the locations of the three top headings at the corresponding date in Fig. 7 are presented in Fig. 8. By combining Fig. 7 with Fig. 8, it can be discovered that the top heading of the middle pilot was always excavated close to or through the monitoring point where the maximum settlement

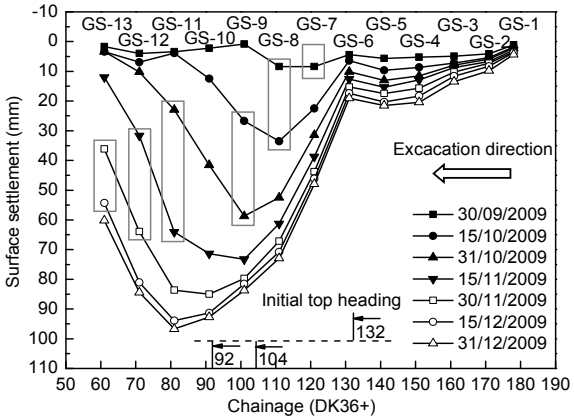

Fig. 7 Longitudinal surface settlements in every half month

increment occurred. For example, the monitoring point GS-9 at DK36+101 had a maximum settlement increment of 32 mm from Oct. 15 to Oct. 31, and Huanzhong Line was excavated from DK36+114 to DK36+98 in the meantime. Therefore, the construction impact of Huanzhong Line rather than Xili Line is highlighted.

The maximum allowable surface settlement is usually set to 35 mm based on abundant tunneling projects with different ground conditions, cover depths, and construction methods using STM in China (Yao and Wang, 2006). In some recently reported projects, the surface settlements were still below this allowable value (Fang *et al*., 2016). However, the tunneling-induced settlement in this study reached a very high level at the end. The measured maximum value was approximately 95 mm, which far exceeded the allowable value. Because the project was constructed under the groundwater table in permeable ground, groundwater seepage was observed on the heading and the inner side of the primary lining during tunneling. The discharge of groundwater was approximately 3–4 $m^3/(d \cdot m)$. The development process of the surface settlement was investigated in the following sections to reveal the influence of groundwater seepage inside Huanzhong Line.

3.3 Development of surface settlements

The progressive developments of surface settlement from GS-1 to GS-13 are plotted against time in Fig. 9. According to the initial positions of the three top headings, the 13 monitoring points can be roughly separated into the following three types: (1) GS-1–GS-6 that mainly reflect the development of post-construction settlement, (2) GS-7–GS-9 that mainly reflect the development of settlement induced by the tunneling of Huanzhong Line, and (3) GS-10–GS-13 that reflect the development of settlement induced by the tunneling of both lines. These developing processes were analyzed based on this categorization.

Fig. 9a shows the settlement histories of GS-1–GS-6, which are taken as post-construction settlement. Settlement measured by these points continued to increase gradually in a basically linear trend

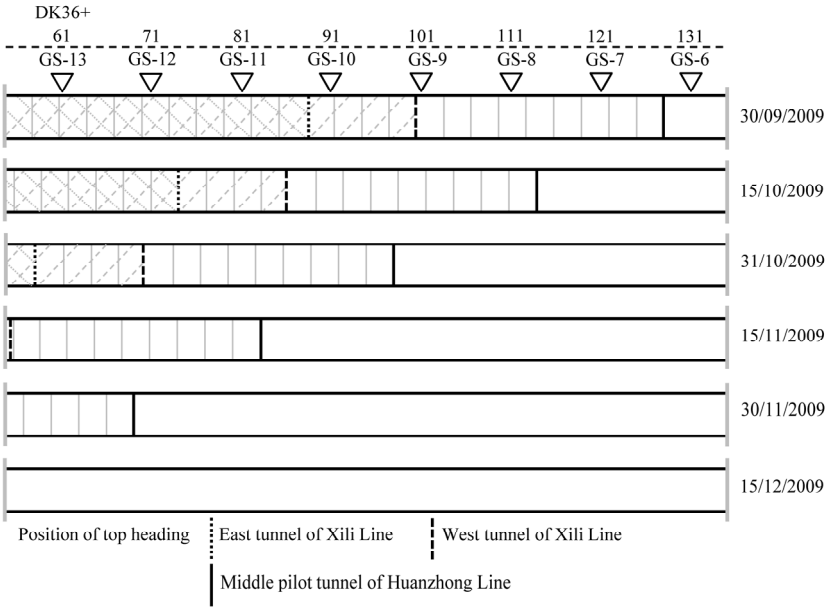

Fig. 8 Locations of top headings in overlapped tunnels

and did not stabilize as time elapsed for nearly 4 months, even after the completion of the secondary lining. The settlement rates were similar at GS-4–GS-6 and gradually declined from GS-4 to GS-1. The maximum settlement of 21.5 mm appeared at GS-5 with an average growth rate of 0.18 mm/d. The post-construction settlement is probably due to the consolidation that lasted for a long time after the groundwater seepage in Huanzhong Line. Creep deformation is also likely to occur in the meantime. The stacked tunnels are mainly located in the completely and severely weathered rock, covered by the sandy clay. Weak rock, such as soft clay, can show obvious creep characteristics, which were verified through laboratory tests (Maranini and Brignoli, 1999; Xu *et al*., 2004). Because the creep deformation may be a dominant part of the total surface settlement after long-term accumulation (Wang *et al*., 2012), regular settlement monitoring is still necessary even after tunneling to avoid potential danger.

Fig. 9b shows the settlement histories of GS-7–GS-9, which primarily present the tunneling-induced settlement of Huanzhong Line. Only the location of the top heading of the middle pilot is plotted here because the distance between each two tunnel headings is constant during simultaneous tunneling. In addition, the dates when the top heading of the middle pilot arrived below each monitoring point are marked by vertical bars. It is evident that surface settlement increased significantly during the tunneling of Huanzhong Line after the construction stoppage. Because GS-9 is the farthest from the top heading of the middle pilot at the beginning of monitoring, the measurements at GS-9 reflect the development process of surface settlement more completely. Taking GS-9 for analysis, the total settlement reached a remarkably high value of 83.7 mm. There was a distinct rapid settlement period with an average rate of 1.57 mm/d, which began 30 d before the arrival of the top heading of the middle pilot and ended 10 d after the departure of the top heading of the right main tunnel. This means that the construction of Huanzhong Line mainly affected the zone $4.0D_H$ ahead of the forefront heading and $1.5D_H$ behind the hindmost heading (D_H represents the height of Huanzhong Line in Fig. 2). In addition, the settlement rate at GS-7–GS-9 dropped to an average value of 0.18 mm/d after the rapid settlement period. This settlement rate was

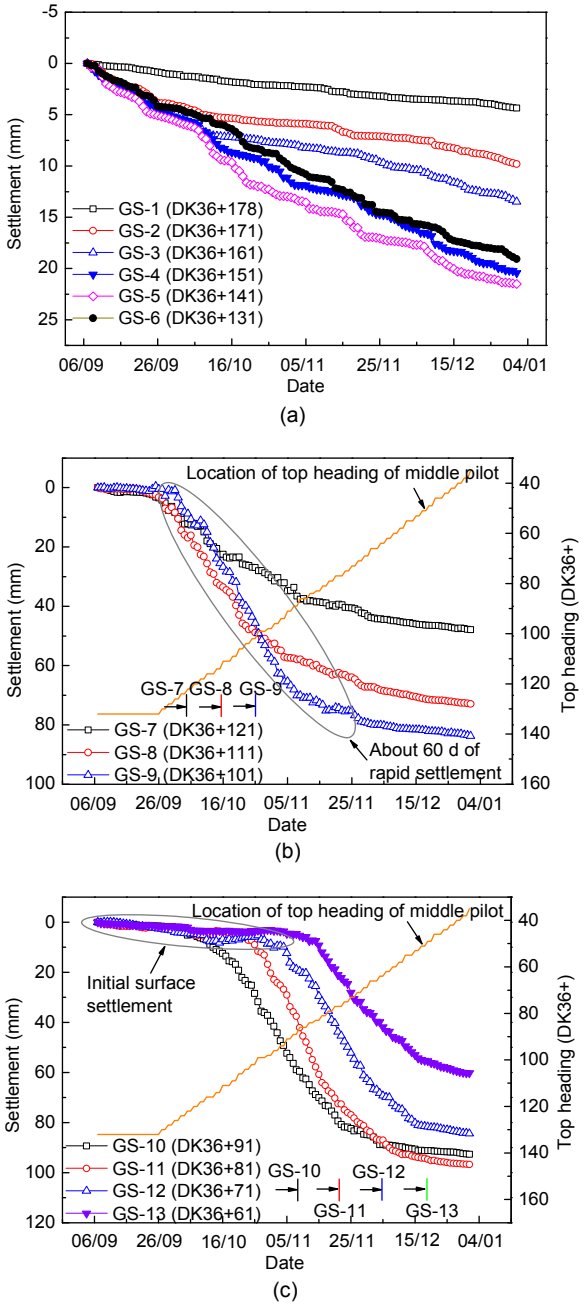

Fig. 9 Progressive development of surface settlements
(a) GS-1–GS-6; (b) GS-7–GS-9; (c) GS-10–GS-13

comparative with that at GS-4–GS-6, which indicates that the influence of tunneling almost vanished.

As mentioned above, tunnel convergence may not be the only reason for such notable surface settlement. First, groundwater seepage inside Huanzhong Line would also contribute. High groundwater level and the medium permeability of sandy clay and weathered rock (10^{-6}–10^{-7} m/s) cause the

groundwater to easily seep. Groundwater inflow continuously occurred through both the heading and the periphery of the double-arched tunnel because the sealing effect of the small pipe grouting and the primary lining seem to be quite limited. As a consequence, the pore pressure declined, and the effective stress increased in the surrounding ground. Consolidation then became a primary factor for the significant surface settlement. Although soil erosion may be accompanied by groundwater seepage, its contribution to the surface settlement is small as no evident erosion was observed during tunneling. Second, owing to the large span of Huanzhong Line, the sequential excavation caused stress redistribution more than once, which intensified both the influence of tunnel convergence and consolidation.

Fig. 9c plots the development processes of surface settlement of GS-10–GS-13. The surface settlement increased very slowly (0.08–0.17 mm/d) in the early days of monitoring, as the headings of Xili Line were excavated through these monitoring points. Owing to the long distance between the headings of Xili Line and Huanzhong Line, it can be considered that the small initial settlement is related only to the tunneling of Xili Line. Because of the implementation of the full-section pre-grouting, the surrounding ground was reinforced, and a good waterproof shell was created around Xili Line. Without groundwater seepage, the surface settlement was well controlled at a level of 3–8 mm. Afterwards, the surface settlement kept growing rapidly as the headings of Huanzhong Line approached and passed. The duration of rapid settlement and the range of the affected zone were similar to those in Fig. 9b.

During the whole monitoring period, the development of the surface settlement was successively caused by the tunneling of Xili Line, the tunneling of Huanzhong Line, and the long-term deformation. The settlement percentages of these three parts were approximately 5%–10%, 75%–85%, and 10%–15%, respectively. The dominating percentage of the second part indicates that groundwater seepage plays an important role in increasing the surface settlement. Consolidation is the main mechanism for the large surface settlement during tunneling in permeable strata. Particular concerns should be given to efficient waterproof measures, such as full-section grouting.

3.4 Fitting of surface settlements

A cumulative frequency function was derived by O'Reilly and New (1982) to describe the surface settlements in a plane parallel to a tunnel by assuming a linear source of volume loss:

$$W = W_{\max}\left[G\left(\frac{x-x_{\mathrm{i}}}{i}\right)-G\left(\frac{x-x_{\mathrm{f}}}{i}\right)\right], \tag{1}$$

where W and $W_{\max}$ are the settlement and maximum settlement in the tunneling direction, respectively; x is the location for the point of interest; i is the trough width parameter that indicates the distance from the inflection point to the tunnel centerline; $G(\cdot)$ represents the cumulative distribution function of a standard normal variable; x_{i} and x_{f} are the initial and final locations of the tunnel face, respectively.

Eq. (1) can also be used to predict the settlement in the longitudinal direction under the conditions of groundwater seepage (Yoo *et al*., 2012). Fig. 10 is a redrawn graph of the settlement history of GS-10 versus the distance to the top heading of the middle pilot. Because the excavation of Huanzhong Line was divided into three tunnels, the measured longitudinal settlement curve was fitted with the sum of three formulas in the form of Eq. (1) according to the principle of superposition (Fillibeck, 2015). Here, i was assumed to be identical for the three formulas. The values of x_{i} and x_{f} in each formula were determined by the location of the corresponding top heading. The distance between two neighboring headings was set as 10 m. The fitted result is shown in Fig. 10 with i of 16.7 m ($2.4D_{\mathrm{H}}$). Eqs. (2) (Clough and Schmidt, 1981) and (3) (Rankin, 1988) are two

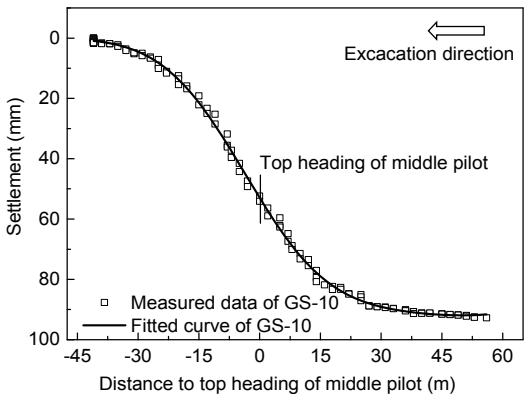

Fig. 10 Curve fitting for settlement history of GS-10

empirical formulas used for predicting i without considering groundwater seepage. By considering Huanzhong Line as the superposition of two intersected arched tunnels, the calculated values of i were 9.7 m and 9.4 m according to Eqs. (2) and (3), respectively. The fitted i was larger than the empirical values, which means that groundwater seepage caused a wider settlement range in the tunneling direction.

$$i = R\left(\frac{H+R}{2R}\right)^{0.8}, \tag{2}$$

$$i = 0.5(H+R), \tag{3}$$

where R and H are the tunnel radius and the thickness of overlying soil, respectively.

3.5 Comparison of surface and crown settlements

Fig. 11 lists the total surface and crown settlements measured in the study region. With respect to Xili Line, the total crown settlement was in the range of 12.5–22.3 mm, and the tunneling-induced surface settlement was approximately 3–8 mm as mentioned above. The surface settlement is smaller than the crown settlement when no groundwater seepage occurs. Regarding Huanzhong Line, the surface settlement can be calculated by subtracting 3–8 mm from the total surface settlement in Fig. 11. Under the groundwater seepage condition, the surface settlement of Huanzhong Line far exceeded its crown settlement (23.1–43.9 mm). The crown settlement accounted for only 25.4%–50.8% of the surface settlement. Because the surface monitoring points GS-8–GS-13 were installed outside the springline of Huanzhong Line, this percentage should be smaller if comparing the crown settlement with the maximum surface settlement near the tunnel center. It is worth mentioning that the ratio of the crown settlement to the surface settlement for this project is below the range of 0.5–1.5 that was summarized from more than 70 projects using STM by Yue *et al.* (2007). The consolidation-caused great gap between the surface settlement and crown settlement is consistent with the observation during the first stage construction of Shenzhen Metro (Zhang and Huang, 2005) and becomes a common tunneling characteristic in the water-rich region of Shenzhen.

4 Finite difference analysis

A 3D fluid-mechanical coupled finite difference analysis was conducted to simulate the simultaneous tunneling process. Compared with the *in-situ* measurements, the influence of groundwater seepage on the significant settlements was verified, and the developments of surface settlement and pore pressure were investigated under different seepage conditions. Based on the actual tunneling process, the advance drainage measure using horizontal boreholes was further considered in the simulation. The effect of advance drainage on surface settlement was studied. Creep behavior was not considered in the numerical

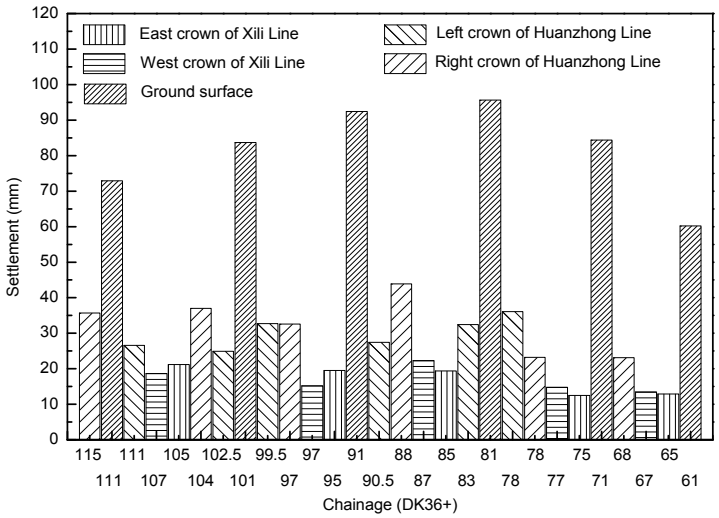

Fig. 11 Comparison between surface settlements and crown settlements

simulation because the main purpose of this study is to highlight the connection between groundwater seepage and surface settlement.

4.1 Finite difference model

The commercial finite difference software program FLAC^{3D} version 3.0 was used for this numerical analysis. The theory of fluid-mechanical interaction can be found in the FLAC^{3D} user's manual (Itasca Consulting Group, 2005). The typical transverse cross section in Fig. 2 was used for creating the 3D numerical model, as shown in Fig. 12. This 3D model consists of 57120 discretized zones and 60329 grid points. The dimensions of the model in the x, y, and z directions are 100 m, 120 m, and 40 m, respectively. The displacement perpendicular to the four vertical boundaries (x=−50 m, x=50 m, y=0, and y=120 m) and the bottom boundary (z=−40 m) were fixed at 0. Regarding the fluid boundary, the original groundwater level was set −3 m below the ground surface. The pore pressures at the four vertical boundaries were restrained equal to the initial values throughout the analysis. This means that groundwater could be drawn through lateral boundaries. An impermeable boundary where pore pressure could freely change was assigned to the water level at z=−3 m and the bottom boundary. The groundwater level was allowed to drawdown towards the tunnel assuming an insufficient amount of rainfall to balance the amount of water flowing into the tunnel.

The behavior of the soil and rock layers was described using an elastic perfectly plastic constitutive model conforming to Mohr–Coulomb failure criterion together with the non-associated flow rule. This model has been widely used in the tunneling modeling (Dias and Kastner, 2013; Xie *et al*., 2016). Geotechnical parameters of different layers listed in Table 1 were used for the analysis. Meanwhile, an isotropic fluid flow model was assigned to the zones considering the soil particle to be incompressible. Fig. 13 plots the zone of pre-grouting and primary lining. Both the full-section grouting and the small pipe grouting were modeled by changing the mechanical properties and the permeability in the pre-grouting zone, which was quoted from Yoo (2005). The primary lining was modeled by the combination of structural shell elements that solve forces and moments and discretized zones with a prescribed permeability (Shin *et al*., 2002). The values of Young's modulus and Poisson's ratio of shotcrete lining are 28 GPa and 0.3, respectively. The shotcrete on the heading of Huanzhong Line was simply modeled by shell elements with a Young's modulus of 10 GPa. Note that the secondary lining was neglected in the simulation because all design loads are supported only by the primary lining in the cases of STM.

The permeability of 6×10^{-9} m/s used by Yoo (2005) implies a perfect waterproof effect in the pre-grouting zones. However, the actual permeability of the small pipe grouting zone or the primary lining

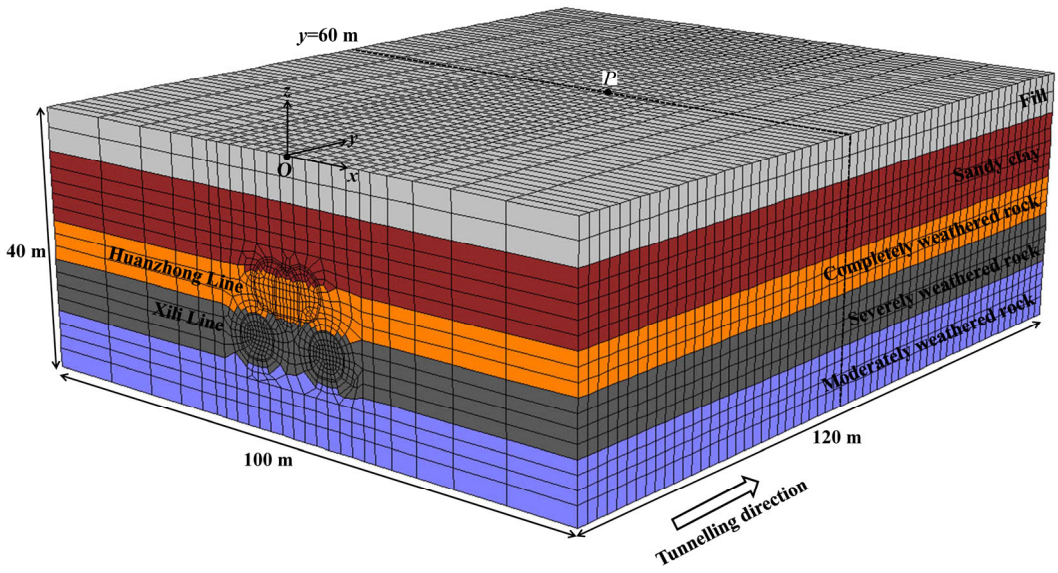

Fig. 12 Finite difference model

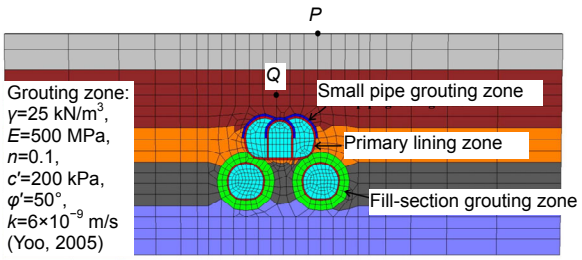

Fig. 13 Middle cross section of numerical model (y=60 m)

varied with the quality of the workmanship. Therefore, two extreme conditions were considered for both the small pipe grouting zone and the primary lining in the simulation. The permeability was set to 6×10^{-9} m/s to model a perfect waterproof effect and was assigned as the original permeability of the strata (Table 1) to represent a very poor waterproof situation. In addition, the permeability of the full-section grouting zone was always assigned as 6×10^{-9} m/s because groundwater inflow into Xili Line could hardly occur with the resistance of a 2 m thick grouting shell. In contrast, the shotcrete on the heading was assumed to show no resistance to groundwater seepage as its thickness (6 cm) is much smaller than that of the primary lining.

The initial stress and pore pressure fields were first established. The simulation of the tunneling process was then carried out according to the practical construction sequences mentioned in Figs. 4 and 5. Note that the distance between two neighboring top headings of Huanzhong Line and the bench length were designated as 10 m and 4 m, respectively. The whole tunneling process was performed by a succession of calculation cycles. Each cycle consists of pre-grouting, excavation, mechanical calculation with the excavation boundary unlined, installation of primary lining, and fluid-mechanical interaction calculation. During each cycle, the excavation length is 2 m, and 100 mechanical calculation steps were executed before installing the shell elements to simulate the temporary stress release of the surrounding ground. The period of the fluid-mechanical calculation is 2 d based on the practical tunneling speed. For the excavation boundary, a zero-pore-pressure boundary was applied to the tunnel heading and periphery to allow the inflow of groundwater. No evident boundary effect appeared in the simulation because the lateral boundaries (x=−50 m and x=50 m) were $7D_H$ from the center of Huanzhong Line.

Advance drainage is a common measure for practical tunneling in permeable strata (Hong *et al.*, 2007). Zingg and Anagnostou (2012; 2013; 2016) have comprehensively studied the effect of advance drainage on the face stability of a deep-buried tunnel. Considering surface settlement becomes an important issue for shallow-buried tunnel conditions, the influence of advance drainage on surface settlements was further investigated based on the same numerical model mentioned above. Fig. 14 illustrates the details of the simulated advance drainage measure, which consists of six horizontal drainage boreholes ahead of the crown of the middle pilot. The length of each drainage borehole is 10 m (about $1.5D_H$). Since the diameter of a drainage borehole (usually 10 cm) is much smaller than the tunnel height, the impact of the borehole deformation on surface settlements was neglected in the simulation. Therefore, the drainage boreholes were simply modeled by applying a prescribed outflow on the interior grid points. The flux of each grid point was estimated to be 0.1 m^3/h by the theoretical model suggested by Goodman *et al.* (1965). Horizontal boreholes were not modeled for the left and right main tunnels, because the middle pilot can be regarded as a drainage pilot tunnel to them.

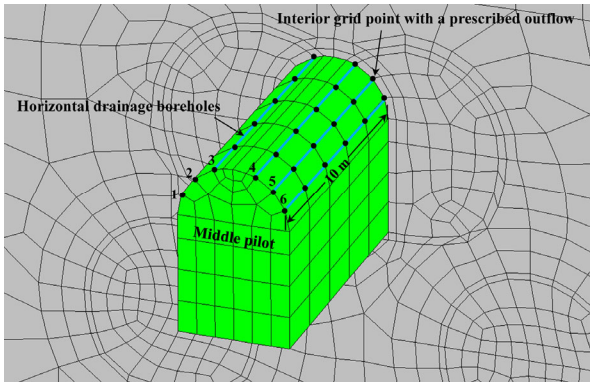

Fig. 14 Details of the simulated horizontal drainage boreholes

4.2 Simulation results of actual tunneling process

The settlement at grid point P (6.14, 60, 0) (Fig. 13) was first compared with the measurements of GS-10 because the relative positions of P and monitoring point GS-10 to Huanzhong Line are the same. Fig. 15 plots the simulated settlement of P and

the measured settlement of GS-10 versus the distance to the top heading of the middle pilot. There are four computed settlement curves 1–4 corresponding to four different seepage conditions I–IV. The developing trend of the computed settlements shows very good agreement with the measured data. Considering the measured data between curve 1 and curve 2, the simulation result matches well with the fact that the primary lining is permeable.

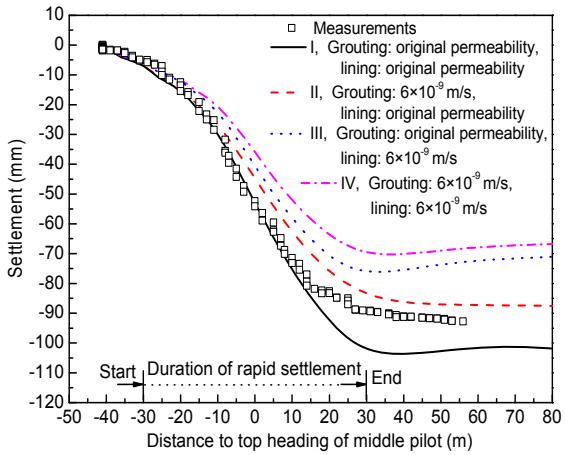

Fig. 15 Computed and measured surface settlements

As shown in Fig. 15, the duration of rapid settlement roughly started when the top heading of the middle pilot was 30 m behind *P* and ended when the heading was 30 m ahead of *P*. This implies that the main affected range induced by groundwater seepage was approximately $4.0D_H$ ahead of the heading of the middle pilot and $1.5D_H$ behind the heading of the right main tunnel. This simulated range is in accordance with that obtained from the measured data. In addition, evident disparities were observed among the four computed settlement curves owing to the permeability differences. Based on the four total settlements, the influence of permeability of the small pipe grouting zone and the shotcrete lining can be quantitatively assessed. Very poor waterproof effects of the small pipe grouting zone and the primary lining can increase by approximately 6%–18% and 29%–43% of the total settlement, respectively. Therefore, the permeability of the primary lining plays a more important role in controlling the surface settlement.

Under the influence of groundwater seepage, Fig. 16 further reveals the pore pressure variation of a representative grid point *Q* (−1.23, 60, −12) that lies $0.5D_H$ above the crown of the middle pilot (Fig. 13). At the start of the tunneling of Huanzhong Line, the pore pressure was almost equal to the initial hydrostatic pressure (90 kPa). This means that the previous tunneling of Xili Line did not change the pore pressure with the assistance of full-section grouting. The pore pressure at *Q* gradually decreased as the top heading of the middle pilot approached. The declining rate reached its maximum value when the top heading was directly beneath *Q*. Comparing curve 1 with the other three curves, it is found that reducing the permeability of the grouting zone and the lining can both effectively lessen the decrease in pore pressure. According to curves 3 and 4, if the permeability of the lining was lower than the original value of the surrounding layers, the pore pressure of *Q* would experience increased recovery after the passing of all headings. Through further investigation of the pore pressure at other grid points, the extent of pore pressure variation is found to be dependent on the locations. For example, the pore pressure at the invert of the middle pilot can be hardly influenced by the permeability of the small pipe grouting zone. Figs. 15 and 16 revealed that the permeability of the grouting zone or the lining influences the surface settlement through changing the pore pressure in the permeable strata. The settlement disparity among the four curves is due to the differences in consolidation settlement.

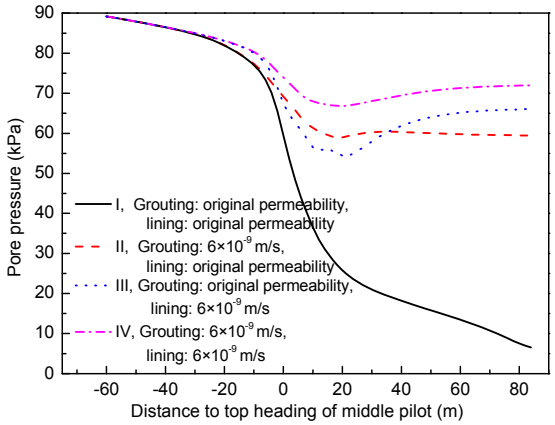

Fig. 16 Computed pore pressure at *Q* (−1.23, 60, −12)

The groundwater seepage also has pronounced effects on the transverse settlement. Figs. 17 and 18 show the contours of the final pore pressure and corresponding vertical displacement, respectively, in the cross section *y*=60 m under the four abovementioned

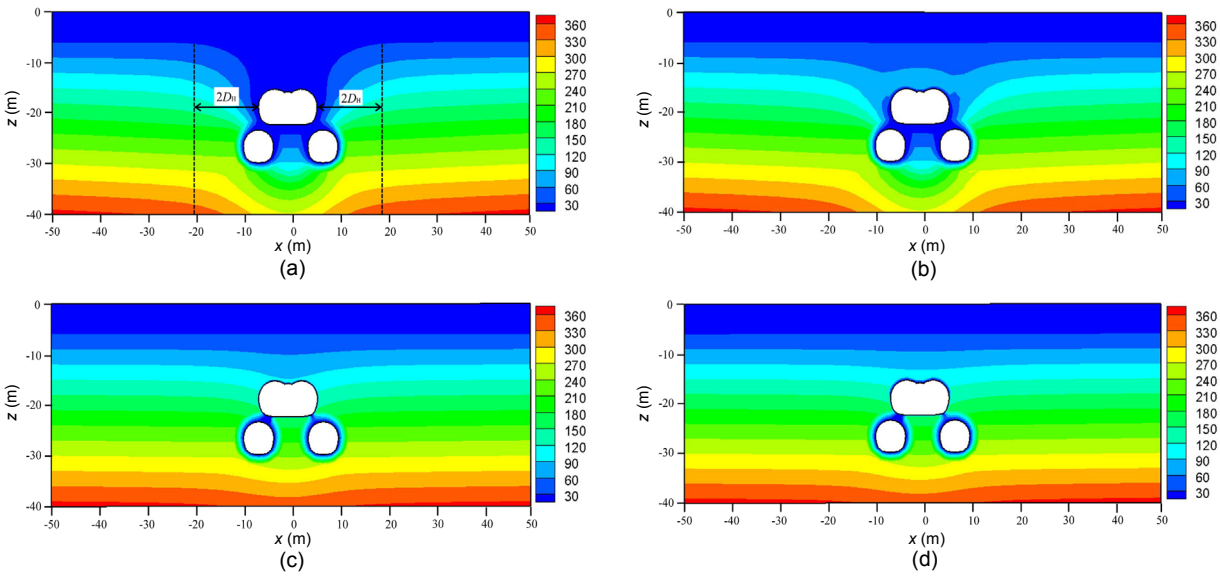

Fig. 17 Distribution of pore pressure (kPa) in the plane y=60 m

(a) Grouting: original permeability, lining: original permeability; (b) Grouting: 6×10^{-9} m/s, lining: original permeability; (c) Grouting: original permeability, lining: 6×10^{-9} m/s; (d) Grouting: 6×10^{-9} m/s, lining: 6×10^{-9} m/s

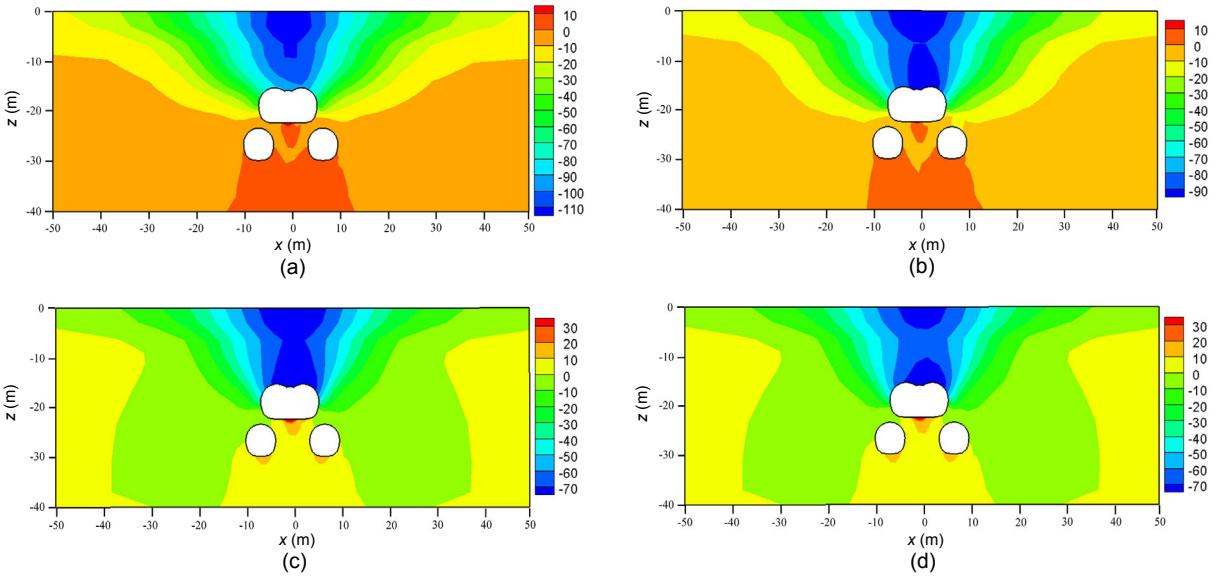

Fig. 18 Distribution of vertical displacement (mm) in the plane y=60 m

(a) Grouting: original permeability, lining: original permeability; (b) Grouting: 6×10^{-9} m/s, lining: original permeability; (c) Grouting: original permeability, lining: 6×10^{-9} m/s; (d) Grouting: 6×10^{-9} m/s, lining: 6×10^{-9} m/s

seepage conditions. As shown in Fig. 17a, the groundwater level drops below the tunnel invert of Huanzhong Line without resistance to groundwater inflow. The pore pressure severely declined from the tunnel center to the location that is approximately $2D_H$ outside the springline. Both the degree and the range of the pore pressure drop decreased with decreasing permeability of the grouting zone or primary lining, which is consistent with the phenomenon in Fig. 16. As shown in Figs. 17c and 17d, the drop in pore pressure in the case of low-permeability lining is quite small owing to the recovery increase in pore pressure mentioned above. With respect to the contours of the vertical displacement in Fig. 18, a considerably wide settlement trough that exceeded the model boundaries can be observed. Owing to the

reduction of the pore pressure drop, the vertical settlement decreased correspondingly in the transverse section. Additionally, integral settlement can be observed between the tunnel crown and the ground surface within the range of the tunnel span. Vertical displacement normally decreases from the crown to the surface in the cases without groundwater seepage (Li *et al.*, 2008), whereas consolidation that occurred in the overlying strata intensified the vertical displacement and caused the integral settlement. The maximum surface settlement was close to or even exceeded the crown settlement. The computed crown settlement is much larger than that in Fig. 11, because the settlement occurred prior to excavation was included.

4.3 Effect of advance drainage

Taking account of advance drainage, tunneling-induced pore pressures and surface settlements were further calculated under the four seepage conditions mentioned above. Fig. 19 compares the contours of pore pressure in the cross section x=−1.23 m without and with the advance drainage boreholes under the seepage condition I. The contours were chosen at the moment when the top heading of the middle pilot was at y=60 m. Due to the drainage action of the six boreholes, pore pressure in front of the top heading decreased remarkably. The pore pressure gradients close to the top heading were also reduced, so that the seepage forces dropped and heading stability was largely improved (Anagnostou and Kovári, 1996). This is also reflected by the maximum horizontal displacements at the top heading of the middle pilot in Table 3. The value was reduced from 152.8 mm to 56.9 mm. However, the displacement reduction at the bottom heading was limited, as the pressure gradient change in front of it was slight. More drainage boreholes can be drilled near the bottom heading to improve the overall face stability. No matter whether the drainage boreholes were used, the maximum horizontal displacements at the headings of the left and right main tunnels were always small owing to the drainage effect of the middle pilot.

The effect of advance drainage on surface settlements is shown in Fig. 20, which compares the computed settlement curves without and with the drainage boreholes under each seepage condition. As the pore pressure dropped earlier under the action of the drainage boreholes (Fig. 19), consolidation settlement occurred in advance resulting in faster development of the surface settlement. Although the use of drainage boreholes could improve the heading stability, the total surface settlement was always slightly larger than that without any drainage boreholes. The settlement differences under the seepage conditions I–IV were 1.3 mm, 2.6 mm, 3.5 mm, and 4.4 mm, respectively. This means the settlement increment caused by the drainage boreholes enlarged as the permeability of the grouting zone and the lining decreased. However, all these settlement increments were less than 10% of the total values, indicating that the effect of drainage boreholes on increasing surface settlement is limited. This is because the drainage boreholes were drilled inside the excavation range of the tunnel and the total decrease in pore pressure

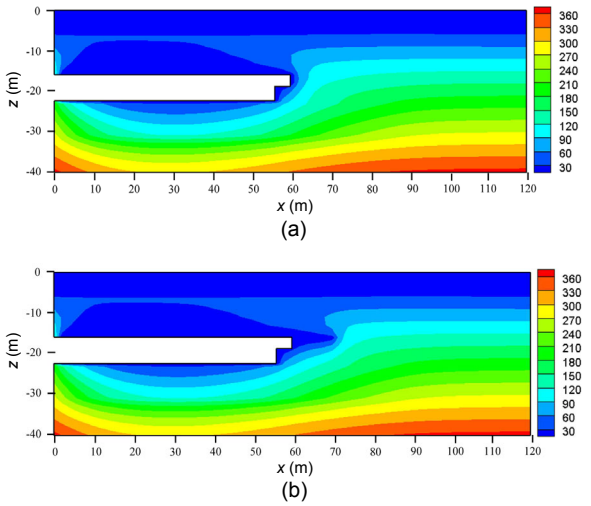

Fig. 19 Distribution of pore pressure (kPa) in the plane x=−1.23 m without (a) and with (b) drainage boreholes

Table 3 Maximum horizontal displacements at the tunnel heading

Huanzhong Line		Maximum horizontal displacement (mm)	
		Without advance drainage	With advance drainage
Middle pilot tunnel	Top heading	152.8	56.9
	Bottom heading	152.3	134.0
Left main tunnel	Top heading	50.4	51.0
	Bottom heading	39.1	37.7
Right main tunnel	Top heading	46.2	47.3
	Bottom heading	44.9	43.2

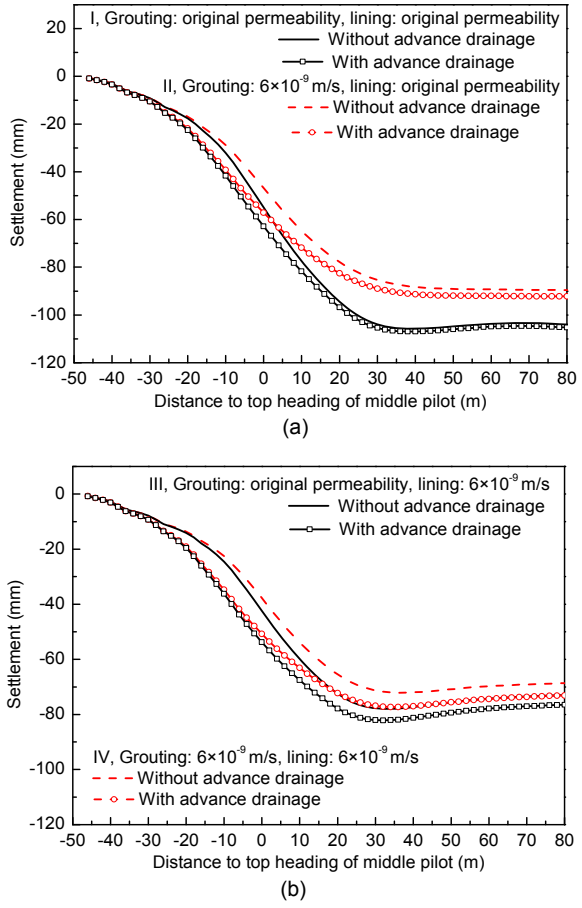

Fig. 20 Computed surface settlements of *P* without and with advance drainage: (a) seepage conditions I and II; (b) seepage conditions III and IV

mainly depended on the seepage conditions of the tunnel.

Although some simplifications were made in the numerical modelling, some qualitative understanding can be drawn from the simulation results. The tunneling-induced surface settlement is significantly influenced by groundwater seepage as a consequence of consolidation. The pre-grouting measure using advanced small pipes cannot effectively control the surface settlement because groundwater inflows from the tunnel heading and periphery. Nevertheless, constructing an impermeable grouting zone and primary lining is still beneficial for reducing the surface settlement. Horizontal drainage boreholes are suggested to be used in conjunction with small pipe grouting, as the advance drainage measure could significantly improve heading stability without much increase in the total surface settlement. This is different from the traditional drainage measure using pumping wells prior to tunneling, which will notably increase the surface settlement (Qi *et al.*, 2010). The layout of drainage boreholes during STM tunneling should be further optimized. Compared with the small pipe grouting, full-section grouting is an excellent measure that prevents seepage and maintains pore pressure unchanged. To avoid excessive surface settlement, the full-section grouting is mandatory during the tunneling in permeable strata, especially for the lower tunnel. If the full-section grouting is not adopted in this project, significant consolidation would occur above the lower tunnel and further be harmful to the structural stability of the upper tunnel. The distance between the upper heading and the lower heading should then be lengthened for the safety of simultaneous tunneling.

5 Conclusions

A case history of remarkable surface settlement induced by simultaneous tunneling with STM in permeable strata was presented in this paper. Field measurements were discussed to recognize the characteristics of surface settlement in relation to groundwater seepage. A 3D fluid-mechanical coupled numerical analysis was then performed to simulate the detailed tunneling process under four different seepage conditions. The following conclusions can be drawn:

1. Groundwater seepage is the main cause of the rapid increase in surface settlement. The contribution of creep deformation to the total surface settlement should also be noticed in the long term. The effect of small pipe grouting is limited in avoiding excessive surface settlement, and the measure of full-section grouting is mandatory, especially for the lower tunnel.

2. Under the influence of groundwater seepage, the affected settlement range for the Huanzhong Line extends approximately $4D_H$ ahead of the forefront heading and ends at $1.5D_H$ behind the hindmost heading. The fitted value of i becomes larger than the empirical values, and the surface settlement can be much greater than the measured crown settlement.

3. The 3D numerical results demonstrate that significant surface settlement is mainly caused by groundwater seepage and is influenced by the

permeability of the small pipe grouting zone and the primary lining. By lowering the permeability, especially the permeability of the lining, the surface settlement can be reduced as the pore pressure drop in the ground is lessened.

4. Due to the seepage inside the Huanzhong Line, the vertical displacement in the transverse section occurs in a very wide range that exceeds the lateral boundaries. Integral settlement arises between the tunnel crown and the ground surface within the range of the tunnel span.

5. The advance drainage measure with horizontal boreholes evidently improves the safety of tunnel headings, and has limited effect on surface settlement. When full-section grouting is not available, it is an alternative measure to be adopted in combination of small pipe grouting during tunneling in permeable strata.

References

Anagnostou, G., 1995. The influence of tunnel excavation on the hydraulic head. *International Journal for Numerical and Analytical Methods in Geomechanics*, **19**(10):725-746. http://dx.doi.org/10.1002/nag.1610191005

Anagnostou, G., 2008. The effect of tunnel advance rate on the surface settlement. Proceedings of the 12th International Conference on Computer Methods and Advances in Geomechanics, p.579-586.

Anagnostou, G., Kovári, K., 1996. Face stability conditions with earth pressure balanced shields. *Tunnelling and Underground Space Technology*, **11**(2):165-173. http://dx.doi.org/10.1016/0886-7798(96)00017-X

Attewell, P.B., Woodman, J.P., 1982. Predicting the dynamics of ground settlement and its derivatives caused by tunnelling in soil. *Ground Engineering*, **15**(8):13-22.

Attewell, P.B., Yeates, J., Selby, A.R., 1986. Soil Movements Induced by Tunnelling and Their Effects on Pipelines and Structures. Blackie & Son Ltd., Glasgow, UK.

Chapman, D.N., Ahn, S.K., Hunt, D.V.L., 2007. Investigating ground movements caused by the construction of multiple tunnels in soft ground using laboratory model tests. *Canadian Geotechnical Journal*, **44**(6):631-643. http://dx.doi.org/10.1139/t07-018

Chen, S.L., Gui, M.W., Yang, M.C., 2012. Applicability of the principle of superposition in estimating ground surface settlement of twin- and quadruple-tube tunnels. *Tunnelling and Underground Space Technology*, **28**:135-149. http://dx.doi.org/10.1016/j.tust.2011.10.005

Clough, G.W., Schmidt, B., 1981. Chapter 8-Design and performance of excavations and tunnels in soft clay. *Developments in Geotechnical Engineering*, **20**:567-634. http://dx.doi.org/10.1016/B978-0-444-41784-8.50011-3

de Farias, M.M., Junior, A.H.M., de Assis, A.P., 2004. Displacement control in tunnels excavated by the NATM: 3-D numerical simulations. *Tunnelling and Underground Space Technology*, **19**(3):283-293. http://dx.doi.org/10.1016/j.tust.2003.11.006

Dias, D., Kastner, R., 2013. Movements caused by the excavation of tunnels using face pressurized shields–analysis of monitoring and numerical modelling results. *Engineering Geology*, **152**(1):17-25. http://dx.doi.org/10.1016/j.enggeo.2012.10.002

Do, N.A., Dias, D., Oreste, P., 2014. Three-dimensional numerical simulation of mechanized twin stacked tunnels in soft ground. *Journal of Zhejiang University-SCIENCE A (Applied Physics & Engineering)*, **15**(11):896-913. http://dx.doi.org/10.1631/jzus.A1400117

Ercelebi, S.G., Copur, H., Ocak, I., 2011. Surface settlement predictions for Istanbul Metro tunnels excavated by EPB-TBM. *Environmental Earth Sciences*, **62**(2):357-365. http://dx.doi.org/10.1007/s12665-010-0530-6

Fang, Q., Zhang, D.L., Wong, L.N.Y., 2011. Environmental risk management for a cross interchange subway station construction in China. *Tunnelling and Underground Space Technology*, **26**(6):750-763. http://dx.doi.org/10.1016/j.tust.2011.05.003

Fang, Q., Zhang, D.L., Wong, L.N.Y., 2012. Shallow tunnelling method (STM) for subway station construction in soft ground. *Tunnelling and Underground Space Technology*, **29**:10-30. http://dx.doi.org/10.1016/j.tust.2011.12.007

Fang, Q., Tai, Q.M., Zhang, D.L., *et al*., 2016. Ground surface settlements due to construction of closely-spaced twin tunnels with different geometric arrangements. *Tunnelling and Underground Space Technology*, **51**:144-151. http://dx.doi.org/10.1016/j.tust.2015.10.031

Fillibeck, J., 2015. Tunnel-induced settlements–analysis of measurements and FE-calculations. Proceedings of the ITA-AITES World Tunnel Congress 2015–Promoting Tunnelling in South East European Region, p.142-143.

Goodman, R.E., Moye, D.G., Schalkwyk, A.V., *et al*., 1965. Groundwater inflows during tunnel driving. *Engineering Geology*, **2**(1):39-56.

Hage Chehade, F., Shahrour, I., 2008. Numerical analysis of the interaction between twin-tunnels: influence of the relative position and construction procedure. *Tunnelling and Underground Space Technology*, **23**(2):210-214. http://dx.doi.org/10.1016/j.tust.2007.03.004

Hefny, A.M., Chua, H.C., Zhao, J., 2004. Parametric studies on the interaction between existing and new bored tunnels. *Tunnelling and Underground Space Technology*, **19**(4-5):471. http://dx.doi.org/10.1016/j.tust.2004.02.074

Hong, E.S., Shin, H.S., Kim, H.M., *et al.*, 2007. Numerical study on horizontal pre-drainage system using horizontal

directional drilling in subsea tunnelling. *Chinese Journal of Rock Mechanics and Engineering*, **26**(S2):3697-3703.

Itasca Consulting Group, 2005. Fast Lagrangian Analysis of Continua in 3 Dimensions. Itasca Consulting Group, Minneapolis, USA.

Li, X.B., Zhang, W., Li, D.Y., *et al*., 2008. Influence of underground water seepage flow on surrounding rock deformation of multi-arch tunnel. *Journal of Central South University of Technology*, **15**(1):69-74. http://dx.doi.org/10.1007/s11771-008-0015-x

Liu, W., Albers, B., Zhao, Y., *et al*., 2016. Upper bound analysis for estimation of the influence of seepage on tunnel face stability in layered soils. *Journal of Zhejiang University-SCIENCE A (Applied Physics & Engineering)*, **17**(11):886-902. http://dx.doi.org/10.1631/jzus.A1500233

Mair, R.J., 1996. Settlement effects of bored tunnels. Proceedings of the 2nd International Symposium on Geotechnical Aspects of Underground Construction in Soft Ground, p.43-53.

Maranini, E., Brignoli, M., 1999. Creep behaviour of a weak rock: experimental characterization. *International Journal of Rock Mechanics and Mining Sciences*, **36**(1):127-138. http://dx.doi.org/10.1016/S0148-9062(98)00171-5

MOR (Ministry of Railways of People's Republic of China), 2005. Code for Design on Tunnel of Railway, TB 10003-2005. MOR, China (in Chinese).

New, B.M., O'Reilly, M.P., 1991. Tunnelling induced ground movements: predicting their magnitude and effects. Proceedings of the 4th International Conference on Ground Movements and Structures, p.671-697.

O'Reilly, M.P., New, B.M., 1982. Settlements above tunnels in the United Kingdom–their magnitude and prediction. Proceedings of Tunnelling' 82, p.173-181.

Peck, R.B., 1969. Deep excavations and tunnelling in soft ground. Proceedings of the 7th International Conference on Soil Mechanics and Foundations, p.225-290.

Qi, T.Y., Gao, B., Tan, D.M., 2010. Influence of metro tunneling in soft clay strata on underground pipeline. *Journal of Southwest Jiaotong University*, **45**(1):45-53 (in Chinese). http://dx.doi.org/10.3969/j.issn.0258-2724.2010.01.008

Rankin, W.J., 1988. Ground movements resulting from urban tunnelling: predictions and effects. *Geological Society, London, Engineering Geology Special Publications*, **5**(1):79-92. http://dx.doi.org/10.1144/GSL.ENG.1988.005.01.06

Shin, J.H., Addenbrooke, T.I., Potts, D.M., 2002. A numerical study of the effect of groundwater movement on long-term tunnel behaviour. *Géotechnique*, **52**(6):391-403. http://dx.doi.org/10.1680/geot.2002.52.6.391

Suwansawat, S., Einstein, H.H., 2007. Describing settlement troughs over twin tunnels using a superposition technique. *Journal of Geotechnical and Geoenvironmental Engineering*, **133**(4):445-468. https://doi.org/10.1061/(asce)1090-0241(2007)133:4(445)

Wang, M.S., 2010. Tunnelling and Underground Engineering Technology in China. China Communications Press, Beijing, China (in Chinese).

Wang, Z.C., Wong, R.C.K., Li, S.C., *et al*., 2012. Finite element analysis of long-term surface settlement above a shallow tunnel in soft ground. *Tunnelling and Underground Space Technology*, **30**:85-92. http://dx.doi.org/10.1016/j.tust.2012.02.010

Xiang, Y.Y., He, S.H., Cui, Z.J., *et al*., 2005. A subsurface "drift and pile" protection scheme for the construction of a shallow metro tunnel. *Tunnelling and Underground Space Technology*, **20**(1):1-5. http://dx.doi.org/10.1016/j.tust.2004.04.001

Xie, X.Y., Yang, Y.B., Mei, J., 2016. Analysis of ground surface settlement induced by the construction of a large-diameter shield-driven tunnel in Shanghai, China. *Tunnelling and Underground Space Technology*, **51**:120-132. http://dx.doi.org/10.1016/j.tust.2015.10.008

Xu, P., Yang, T.Q., Zhou, H.M., 2004. Study of the creep characteristics and long-term stability of rock masses in the high slopes of the TGP ship lock, China. *International Journal of Rock Mechanics and Mining Sciences*, **41**(S1):261-266. http://dx.doi.org/10.1016/j.ijrmms.2004.03.051

Yao, X.D., Wang, M.S., 2006. Statistic analysis of guideposts for ground settlement induced by shallow tunnel construction. *Chinese Journal of Rock Mechanics and Engineering*, **25**(10):2030-2035 (in Chinese). http://dx.doi.org/10.3321/j.issn:1000-6915.2006.10.013

Yoo, C., 2005. Interaction between tunnelling and groundwater –numerical investigation using three dimensional stress-pore pressure coupled analysis. *Journal of Geotechnical and Geoenvironmental Engineering*, **131**(2):240-250. https://doi.org/10.1061/(asce)1090-0241(2005)131:2(240)

Yoo, C., Lee, Y.J., Kim, S.H., *et al*., 2012. Tunnelling-induced ground settlements in a groundwater drawdown environment–a case history. *Tunnelling and Underground Space Technology*, **29**:69-77. http://dx.doi.org/10.1016/j.tust.2012.01.002

Yue, G.X., He, P., Cai, W., 2007. Statistic analysis of stratum deformation during tunnel excavation. *Chinese Journal of Rock Mechanics and Engineering*, **26**(S2):3793-3803 (in Chinese).

Zhang, C.P., Zhang, D.L., Wang, M.S., *et al*., 2008. Analysis of stratum deformation induced by overlapping tunnels construction in shallow depth. *Chinese Journal of Rock Mechanics and Engineering*, **27**(S1):3244-3250 (in Chinese).

Zhang, D.L., Huang, J., 2005. Analysis and prediction of vault

crown settlement in metro tunneling at shallow depth. *Chinese Journal of Rock Mechanics and Engineering*, **24**(10):1703-1707 (in Chinese). http://dx.doi.org/10.3321/j.issn:1000-6915.2005.10.012

Zingg, S., Anagnostou, G., 2012. The effects of advance drainage on face stability in homogeneous ground. Proceedings of the ITA-AITES World Tunnel Congress 2012–Tunnelling and Underground Space for a Global Society.

Zingg, S., Anagnostou, G., 2013. Effect of tunnel diameter on the efficiency of advance drainage with respect to face stability. Proceedings of the International Symposium on Tunnelling and Underground Space Construction for Sustainable Development, p.277-280.

Zingg, S., Anagnostou, G., 2016. An investigation into efficient drainage layouts for the stabilization of tunnel faces in homogeneous ground. *Tunnelling and Underground Space Technology*, **58**:49-73. http://dx.doi.org/10.1016/j.tust.2016.04.004

中文概要

题　目：渗透性地层中隧道施工引起的地表沉降——以深圳地铁为例

目　的：在城市地铁的建设过程中，地下水渗流对地表沉降存在较大影响。然而，渗透性地层中浅埋暗挖法施工的案例报道较少，地表沉降规律尚不明晰。本文以深圳地铁 5 号线和 7 号线重叠段工程为例，详细分析在渗流作用下浅埋暗挖法施工引起的地表沉降特征以及小导管注浆区和初支衬砌渗透性对地表沉降的影响，并进一步研究超前排水措施在沉降控制方面的作用。

创新点：1. 系统分析了富水渗透性地层中浅埋暗挖隧道施工引起的地表沉降的发展过程以及沉降特征；2. 验证了三维流固耦合数值模型模拟富水环境下重叠隧道施工过程的可行性；3. 研究了小导管注浆区、初支衬砌的渗透性和超前排水措施对地表沉降的影响。

方　法：1. 结合隧道施工方案和地表沉降监测数据，分析渗流作用下的地表沉降特征（包括沉降影响范围、沉降槽宽度以及与拱顶沉降的关系等）；2. 通过三维流固耦合数值模型，研究小导管注浆区和初支衬砌渗透性对地表沉降以及地层孔压变化过程的影响；3. 通过模拟掌子面前方水平排水孔，研究超前排水措施对掌子面稳定性和地表沉降发展的影响。

结　论：1. 对于渗透性地层中的浅埋暗挖隧道工程，地下水渗流引起的固结效应是地表沉降量以及沉降范围大幅增长的主要原因。2. 全断面注浆能够很好地控制地表沉降，而小导管注浆的效果则十分有限。3. 降低小导管注浆区的渗透性，尤其是初支衬砌的渗透性，可以减少地层孔压的下降程度，进而降低地表沉降。4. 打设超前水平排水孔可以显著提高掌子面稳定性，却对地表沉降影响有限；当无法进行全断面注浆时，推荐采取小导管注浆与超前排水相结合的方式施工。

关键词：地表沉降；浅埋暗挖法；地下水渗流；预注浆；超前排水；流固耦合分析